14. M. A. Ward, P. S. Burgoyne, *Biol. Reprod.* **74**, 652 (2006).
15. M. Gomendio, A. H. Harcourt, E. R. S. Roldan, in *Sperm Competition and Sexual Selection*, T. R. Birkhead, A. P. Møller, Eds. (Academic Press, London, 1998).
16. J. Carranza, P. Fernandez-Llario, M. Gomendio, *Ethology* **102**, 793 (1996).
17. B. T. Preston, I. R. Stevenson, J. M. Pemberton, K. Wilson, *Nature* **409**, 681 (2001).
18. M. Gomendio, T. H. Clutton-Brock, S. D. Albon, F. E. Guinness, M. J. A. Simpson, *Nature* **343**, 261 (1990).
19. Empresa Medianilla allowed work at Finca Las Lomas. Funding was provided by Ministerio de Ciencia y Tecnologia, Ministerio de Educacion y Ciencia, European Regional Development Fund, and Instituto Nacional de Investigacion y Tecnologia Agraria. A.F.M. was supported by a studentship from MCYT, and A.J.S. and M.R.F.-S. received support from JCCM. We thank A. Cockburn, J. M. Cummins, C. LaMunyon, E. Martínez, and J. M. Vázquez for helpful discussions.

Supporting Online Material
www.sciencemag.org/cgi/content/full/314/5804/1445/DC1
Materials and Methods
References

26 July 2006; accepted 26 October 2006
10.1126/science.1133064

WNT and DKK Determine Hair Follicle Spacing Through a Reaction-Diffusion Mechanism

Stefanie Sick,[1] Stefan Reinker,[2]* Jens Timmer,[2] Thomas Schlake[1]†

Mathematical reaction-diffusion models have been suggested to describe formation of animal pigmentation patterns and distribution of epidermal appendages. However, the crucial signals and in vivo mechanisms are still elusive. Here we identify WNT and its inhibitor DKK as primary determinants of murine hair follicle spacing, using a combined experimental and computational modeling approach. Transgenic DKK overexpression reduces overall appendage density. Moderate suppression of endogenous WNT signaling forces follicles to form clusters during an otherwise normal morphogenetic program. These results confirm predictions of a WNT/DKK-specific mathematical model and provide in vivo corroboration of the reaction-diffusion mechanism for epidermal appendage formation.

The development of regularly arranged body parts has long fascinated experimental biologists and theoreticians alike. One area of long-standing debate has been the formation of epidermal appendages such as feathers and hairs. Theoretical models have provided seemingly simple solutions to complex developmental processes (*1*); in order to achieve regular patterns, the reaction-diffusion (RD) hypothesis of Alan Turing postulates a pair of activator and inhibitor with special characteristics (*2*) [supporting online material (SOM) text 1]. However, it remains largely unclear whether such predictions can be substantiated in molecular and mechanistic terms (*3*). Because canonical WNT signaling is essential for the induction of hair and feather follicles (*4, 5*) and forced stimulation of this pathway is sufficient to induce supernumerous appendages (*6, 7*), the pathway represents an appealing candidate for the primary signal that dictates follicle distribution. Here we set out to analyze its role in hair follicle arrangement by verifying predictions of a biologically adapted RD model.

The WNT pathway is active from the earliest stages of follicular development (*5, 8*) (Fig. 1A). Expression of the WNT inhibitor *Dkk1* is directly controlled by secreted WNTs (*9, 10*). Further aspects of this pathway and the RD mechanism are discussed in SOM text 2 and fig. S1. In developing murine skin, mesenchymal *Dkk1* expression is found adjacent to the early hair follicle bud (*5*) (Fig. 1B), whereas *Dkk4*, a further functional inhibitor of WNT signaling (*11, 12*), shows strong epithelial expression at discrete loci before hair placode formation (Fig. 1C). Weak expression in the early hair follicle bud indicates that *Dkk4* expression marks the forming follicle (Fig. 1C). Five LEF/TCF consensus binding motifs are found within 700 base pairs (bp) upstream of the transcriptional start site of *Dkk4*, and regulation of the promoter by the canonical WNT signaling pathway was suggested by transfection studies (Fig. 1D). Hence, the available data support the role of WNT and DKK as primary determinants of hair follicle spacing patterns.

If WNTs and WNT inhibitor(s) represent the two components required by the RD hypothesis, it should be possible to derive, from a WNT/DKK-specific RD model (SOM text 3), predictions about the outcome of experimental alterations of activating and inhibitory functions.

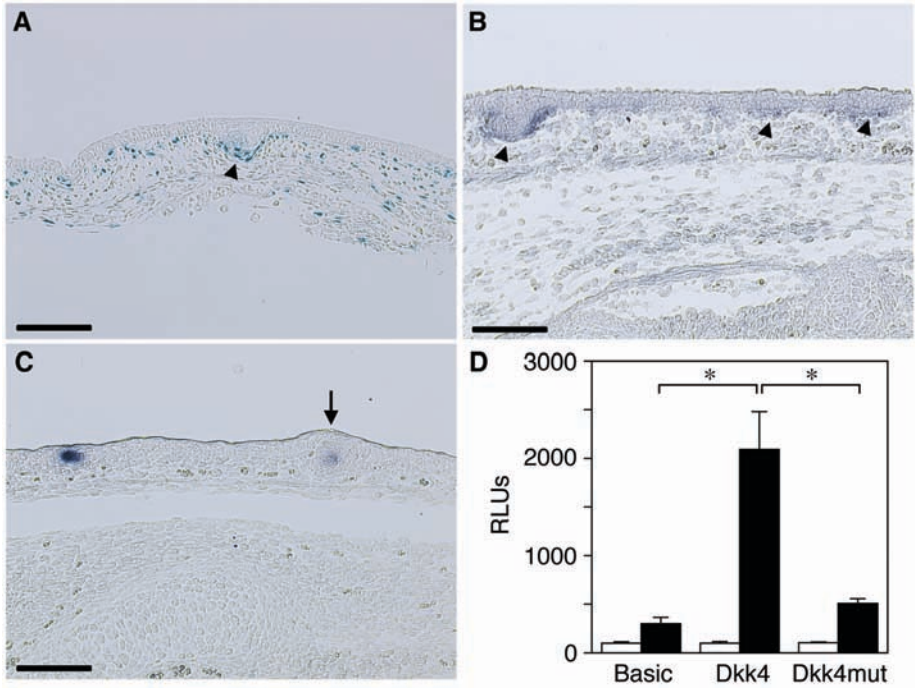

Fig. 1. WNT signaling and expression of *Dkk* genes are associated with hair follicle formation. (**A**) WNT signaling in mesenchymal cells is associated with developing hair follicles (arrowhead). BATgal mice harboring a WNT-responsive *lacZ* gene were used as a reporter. (**B**) Mesenchymal *Dkk1* expression adjacent to epithelial placodes and buds (arrowheads). (**C**) Strong epithelial *Dkk4* expression at discrete loci prior to hair placode formation. Expression rapidly declines after follicle budding (arrow). (A to C) Scale bars, 100 μm. (**D**) Reporter gene expression [relative light units (RLUs) ± SEM] after endogenous (white) and stimulated (black) canonical WNT signaling. *$P < 0.0001$ (*t* test) for stimulated WNT signaling (black columns).

[1]Max-Planck Institute of Immunobiology, Stuebeweg 51, 79108 Freiburg, Germany. [2]Institut für Physik, Universität Freiburg, Hermann-Herder-Strasse 3, 79104 Freiburg, Germany.

*Present address: Novartis Institutes for Biomedical Research, Basel, Switzerland.

†To whom correspondence should be addressed. E-mail: schlake@immunbio.mpg.de

Our computational modeling showed that moderate overexpression of activator during either the initial or a subsequent inductive wave increases follicular density (Fig. 2, A and B). By contrast, strong overexpression of activator completely disrupts the patterning process. Moderate overexpression of inhibitor during the initial inductive wave increases the interfollicular spacing (Fig. 2A). In line with the prediction of defective pattern formation after further enhancement of inhibitor expression, hair and feather follicle induction is indeed blocked in the presence of strong *Dkk1* expression (*4, 5*); however, the role of WNTs in appendage formation and patterning is still contentious. During a subsequent inductive wave, increased inhibitor expression blocks the development of new follicles in the interfollicular space (Fig. 2B). In addition, excess inhibitor gives rise to ringlike zones of high activator levels around preexisting appendages (Fig. 2B). If levels of activator above a threshold

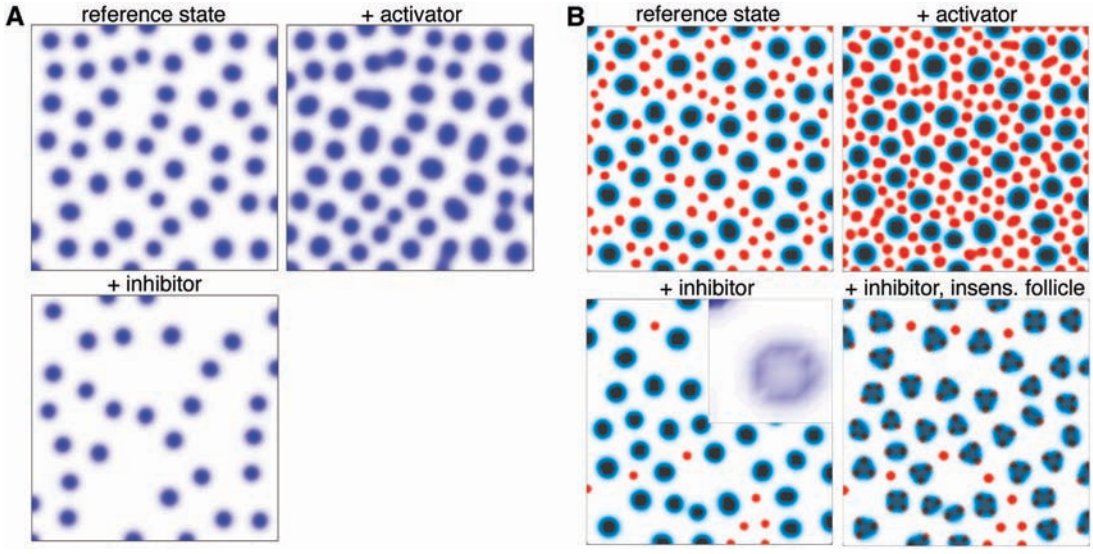

Fig. 2. A WNT/DKK-specific model of a reaction-diffusion system predicts changes in epidermal appendage distribution after transgenic interference with endogenous signaling. Diagrams for excess activator or inhibitor production correspond to moderate overexpression that was restricted to the forming appendages. (**A**) Modeling of the first inductive wave. The calculated distribution of activator is shown for a 100 × 100 area (arbitrary units). (**B**) Modeling of a subsequent inductive wave. The first wave is shown in blue, the second in red. The calculated distribution of activator is depicted for a 200 × 200 area. The inset reflects the difference in activator distribution between second and first inductive wave for a first wave follicle. An activator and inhibitor insensitivity of first wave follicles might reflect the in vivo situation most closely.

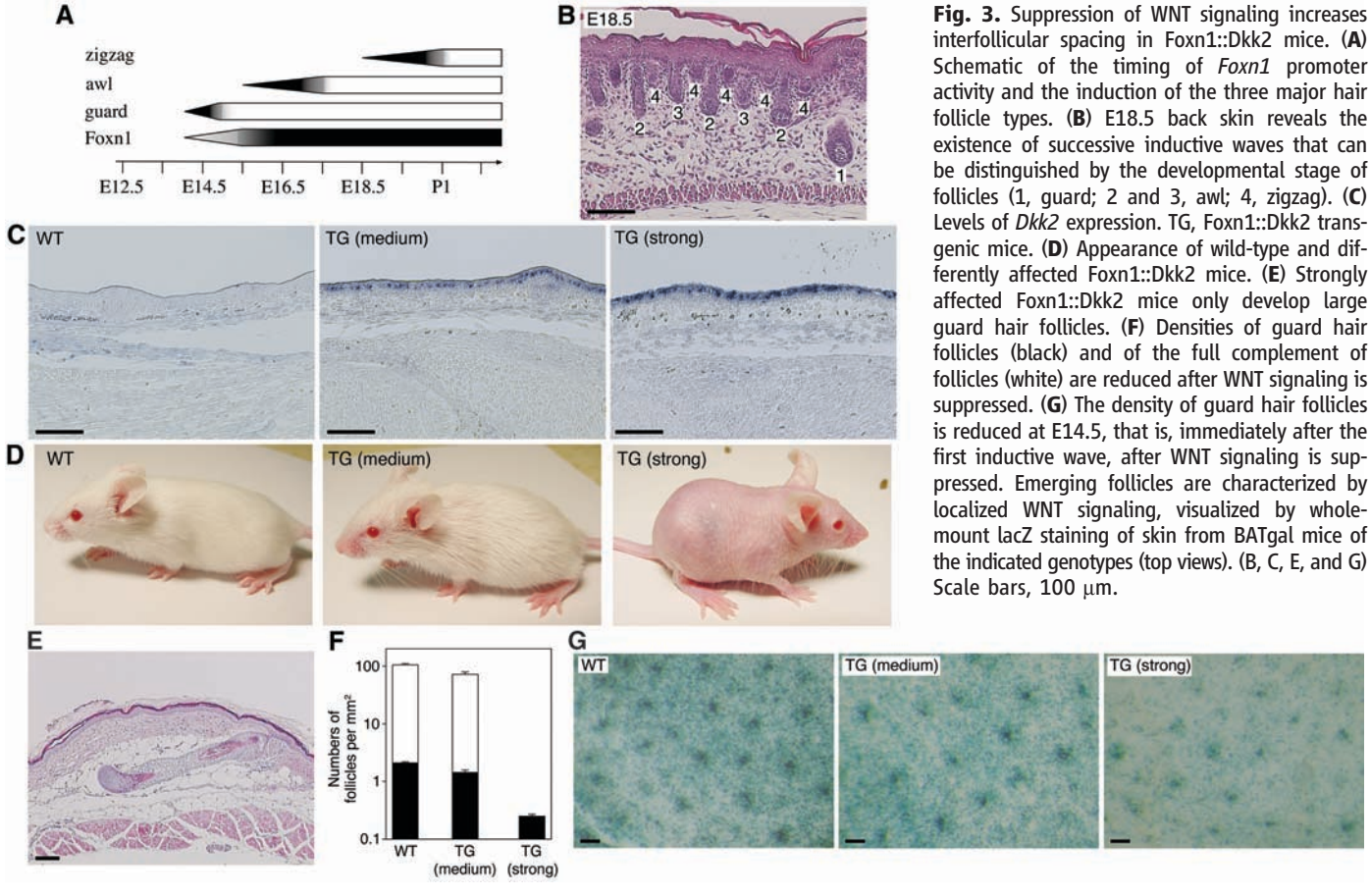

Fig. 3. Suppression of WNT signaling increases interfollicular spacing in Foxn1::Dkk2 mice. (**A**) Schematic of the timing of *Foxn1* promoter activity and the induction of the three major hair follicle types. (**B**) E18.5 back skin reveals the existence of successive inductive waves that can be distinguished by the developmental stage of follicles (1, guard; 2 and 3, awl; 4, zigzag). (**C**) Levels of *Dkk2* expression. TG, Foxn1::Dkk2 transgenic mice. (**D**) Appearance of wild-type and differently affected Foxn1::Dkk2 mice. (**E**) Strongly affected Foxn1::Dkk2 mice only develop large guard hair follicles. (**F**) Densities of guard hair follicles (black) and of the full complement of follicles (white) are reduced after WNT signaling is suppressed. (**G**) The density of guard hair follicles is reduced at E14.5, that is, immediately after the first inductive wave, after WNT signaling is suppressed. Emerging follicles are characterized by localized WNT signaling, visualized by whole-mount lacZ staining of skin from BATgal mice of the indicated genotypes (top views). (B, C, E, and G) Scale bars, 100 μm.

determine where appendages form, this suggests the possibility of follicle cluster formation. The ringlike zones of high activator levels are converted to discrete spots (Fig. 2B) if preexisting follicles become insensitive to activator and inhibitor (SOM text 4). Thus, moderate overexpression of inhibitor by the appendages predicts a quantitative as well as a qualitative read-out: The number of follicles is reduced, and their distribution is changed.

We used transgenic expression of inhibitor during hair follicle formation to experimentally test these theoretical predictions (Fig. 3 and SOM text 5 and fig. S2). In mouse, temporally well defined successive waves of induction during embryogenesis and early postnatal life give rise to three major hair follicle types (designated guard, awl, and zigzag) (*13*) (Fig. 3A). In compliance with the model, new follicles are initiated in between previously induced appendages (Fig. 3B). We analyzed four Foxn1::Dkk2 mouse lines in detail, and their phenotype was correlated to the level of transgene expression (Fig. 3, C and D). At high levels of ectopic *Dkk2* mRNA, mice appeared almost hairless; at lower levels, the hair coat is present but structurally abnormal (Fig. 3D). Suppression of hair follicle formation at high levels of *Dkk2* expression is consistent with previous results for *Dkk1* (*5*) and conforms to the prediction of our computational modeling. However, guard hair follicle induction still took place even in severely affected mice (Fig. 3, D and E) because of the delayed onset of *Foxn1* promoter activation relative to guard hair follicle induction (Fig. 3A and fig. S2).

The number of follicles per square millimeter is reduced by about 30% in adult Foxn1::Dkk2 (medium) mice (Fig. 3F). Regarding the first inductive wave that gives rise to guard hair follicles, a similar reduction is evident (Fig. 3F). In Foxn1::Dkk2 (strong) mice, which only develop guard hair follicles, the density is further reduced (Fig. 3F). The emergence of hair follicle buds is accompanied by localized WNT signaling in mesenchymal cells of the prospective dermal papilla (Fig. 1A). As expected, the density of these cell clusters is reduced in Foxn1::Dkk2 transgenic mice (Fig. 3G). However, we could not detect any difference between mice with high and medium mRNA levels. Thus, the significant decrease of guard hair follicle density in Foxn1::Dkk2 (strong) as compared with Foxn1::Dkk2 (medium) mice suggests the existence of more than one inductive wave for guard hair follicles; apparently, all but the first wave are blocked by strong transgene expression. For the first inductive wave, the results confirm the predictions of our model with respect to the quantitative effects of inhibitor overexpression.

As suggested by our simulations, WNT and DKK proteins may control the natural increase of follicle density during subsequent inductive waves (Fig. 2B and SOM text 6 and figs. S3 and S4). In order to investigate inhibitor effects on these waves, we next examined transgenic mice with an abnormal hair coat in more detail. These mice are characterized by a misdistribution of hair shafts. Whereas emerging hair shafts are almost evenly distributed over the skin surface in wild-type mice, bundles of hair shafts are separated by large areas of interfollicular epidermis in Foxn1::Dkk2 mice (Fig. 4A). Histological sections confirmed that usually more than three follicles are tightly clustered in transgenic mice (Fig. 4B); all follicles within a cluster gave rise to bona fide hair shafts. By contrast, follicles are clearly separated from each other in wild-type skin (Fig. 4B). Strong follicle clustering was also observed in Foxn1::Dkk1 mice (fig. S5), which corroborated its independence of the inhibitor's identity. A ringlike pattern of WNT signal-receiving cells around preexisting follicles confirms the model's prediction for activator distribution and indicates an initiation of cluster formation at about embryonic day 17.5 (E17.5) (Fig. 4C). Unequivocal morphological indications of hair follicle cluster formation were observed at E18.5 and postnatal

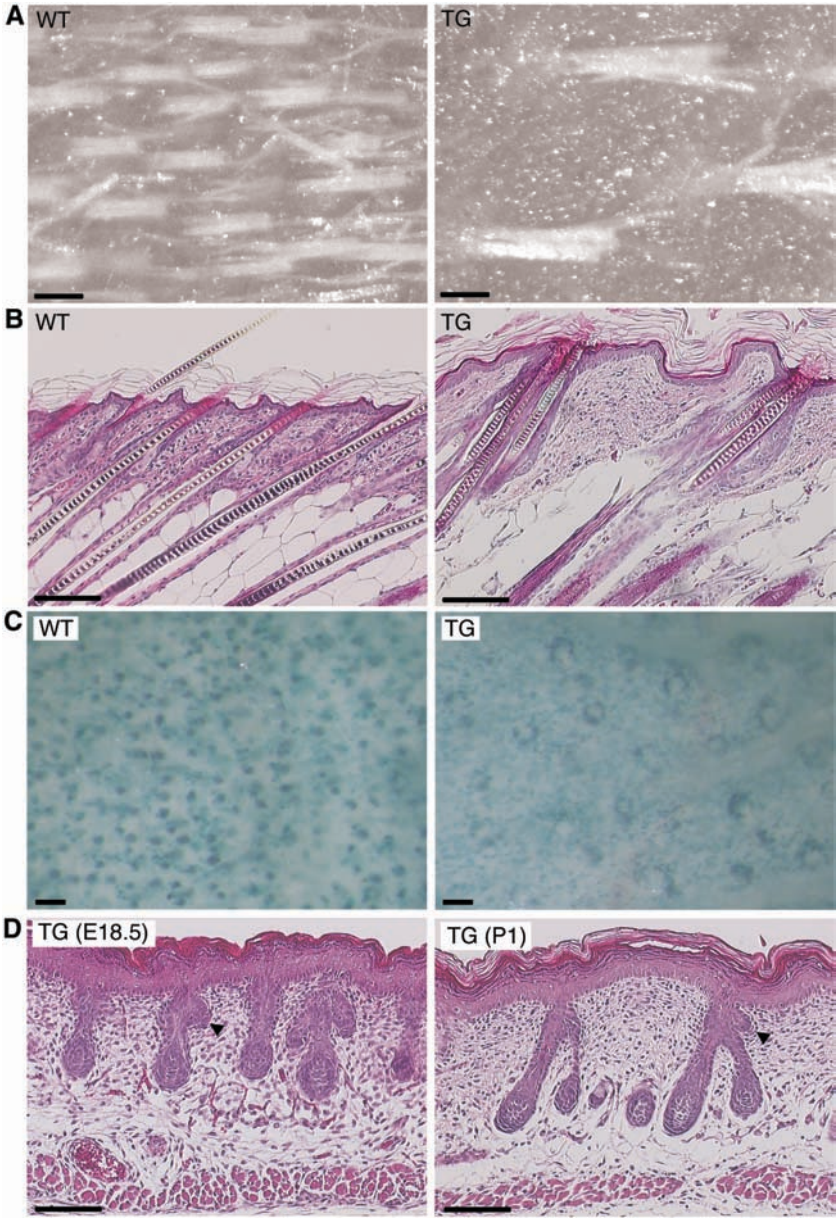

Fig. 4. A normal sequence of inductive waves gives rise to hair follicle clusters after moderate suppression of WNT signaling. (**A**) Hair distribution on the back of wild-type and Foxn1::Dkk2 mice. (**B**) Hair follicle distribution in the back skin of 10-day-old wild-type and Foxn1::Dkk2 animals. (**C**) Aberrant distribution of WNT signal–receiving cells in Foxn1::Dkk2 mice at E17.5. Canonical WNT signaling is visualized by whole-mount lacZ staining of back skin from BATgal mice of the indicated genotypes (top views). (**D**) New follicles (arrowheads) emerge at E18.5 and P1 in Foxn1::Dkk2 mice. All scale bars, 100 μm.

day 1 (P1) (Fig. 4D and fig. S6). Thus, hair follicle clusters in Foxn1::Dkk2 mice form during a normal inductive program by misdistribution of the normal complement of epidermal appendages (Fig. 4D and SOM text 7 and fig. S6).

We note that further signaling pathways are involved in interfollicular patterning. Studies on feather development demonstrated that fibroblast growth factors (FGFs) promote follicle formation, whereas BMP and EGF signaling confers interfollicular fate (*14, 15*). Because these pathways appear to be downstream of WNT signaling and exert feedback control (*5, 14, 16–19*), we propose that they mainly mediate and modulate WNT signals, thereby contributing to the stabilization and refinement of the patterning process. Indeed, ablation of the BMP receptor IA appears to have no major impact on hair follicle induction and distribution (*20*). However, suppression of BMP signaling that may reduce *Dkk1* expression (*19*) causes an increase in hair follicle density (*21*), consistent with our simulations (fig. S3C). Given that LEF1 plays an important role in WNT signaling, which controls ectodysplasin signals (*5, 22*), our results may also explain the misdistribution of follicles in *EdaA1* and *Lef1* transgenic mice (*23, 24*). However, a more sophisticated systems biology approach will be needed in the future to include the full complexity and dynamics of the WNT signaling pathway (*25*) in a model of interfollicular patterning. In conclusion, our combined experimental and computer modeling approach presents compelling evidence for WNT signaling and a reaction-diffusion mechanism as key determinants of hair follicle spacing patterns.

References and Notes

1. K. Amonlirdviman *et al.*, *Science* **307**, 423 (2005).
2. A. Turing, *Philos. Trans. R. Soc. London B Biol. Sci.* **237**, 37 (1952).
3. S. Kondo, R. Asai, *Nature* **376**, 765 (1995).
4. C. H. Chang *et al.*, *Mech. Dev.* **121**, 157 (2004).
5. T. Andl, S. T. Reddy, T. Gaddapara, S. E. Millar, *Dev. Cell* **2**, 643 (2002).
6. S. Nonchev *et al.*, *Development* **122**, 543 (1996).
7. U. Gat, R. DasGupta, L. Degenstein, E. Fuchs, *Cell* **95**, 605 (1998).
8. S. Reddy *et al.*, *Mech. Dev.* **107**, 69 (2001).
9. A. Niida *et al.*, *Oncogene* **23**, 8520 (2004).
10. M. N. Chamorro *et al.*, *EMBO J.* **24**, 73 (2005).
11. V. E. Krupnik *et al.*, *Gene* **238**, 301 (1999).
12. B. Mao, C. Niehrs, *Gene* **302**, 179 (2003).
13. F. W. Dry, *J. Genet.* **16**, 287 (1926).
14. H. S. Jung *et al.*, *Dev. Biol.* **196**, 11 (1998).
15. R. Atit, R. A. Conlon, L. Niswander, *Dev. Cell* **4**, 231 (2003).
16. K. Kratochwil, J. Galceran, S. Tontsch, W. Roth, R. Grosschedl, *Genes Dev.* **16**, 3173 (2002).
17. K. Kratochwil, M. Dull, I. Farinas, J. Galceran, R. Grosschedl, *Genes Dev.* **10**, 1382 (1996).
18. C. Jamora, R. DasGupta, P. Kocieniewski, E. Fuchs, *Nature* **422**, 317 (2003).
19. L. Grotewold, U. Ruther, *EMBO J.* **21**, 966 (2002).
20. K. Kobielak, H. A. Pasolli, L. Alonso, L. Polak, E. Fuchs, *J. Cell Biol.* **163**, 609 (2003).
21. M. Plikus *et al.*, *Am. J. Pathol.* **164**, 1099 (2004).
22. J. Behrens *et al.*, *Nature* **382**, 638 (1996).
23. T. Mustonen *et al.*, *Dev. Biol.* **259**, 123 (2003).
24. P. Zhou, C. Byrne, J. Jacobs, E. Fuchs, *Genes Dev.* **9**, 700 (1995).
25. R. DasGupta, A. Kaykas, R. T. Moon, N. Perrimon, *Science* **308**, 826 (2005).

26. We thank B. Hammerschmidt for her excellent technical help; B. Kanzler, E. Huber, and J. Wersing for producing transgenic mice; C. Bleul and T. Boehm for the *Foxn1* promoter construct; C. Niehrs for murine *Dkk1* cDNA; R. Kemler for *Lef1* and β-catenin expression plasmids; and T. Boehm for helpful discussions and comments on the manuscript.

Supporting Online Material

www.sciencemag.org/cgi/content/full/1130088/DC1
Materials and Methods
SOM Text
Figs. S1 to S6
References

5 May 2006; accepted 18 October 2006
Published online 2 November 2006;
10.1126/science.1130088
Include this information when citing this paper.

Structural Basis for Ribosome Recruitment and Manipulation by a Viral IRES RNA

Jennifer S. Pfingsten, David A. Costantino, Jeffrey S. Kieft*

Canonical cap–dependent translation initiation requires a large number of protein factors that act in a stepwise assembly process. In contrast, internal ribosomal entry sites (IRESs) are *cis*-acting RNAs that in some cases completely supplant these factors by recruiting and activating the ribosome using a single structured RNA. Here we present the crystal structure of the ribosome-binding domain from a Dicistroviridae intergenic region IRES at 3.1 angstrom resolution, providing a view of the prefolded architecture of an all-RNA translation initiation apparatus. Docking of the structure into cryo–electron microscopy reconstructions of an IRES-ribosome complex suggests a model for ribosome manipulation by a dynamic IRES RNA.

In eukaryotes, there are two known mechanisms for the initiation of protein synthesis (Fig. 1A). The canonical mechanism requires a modified nucleotide cap on the 5′ end of the mRNA, which is recognized by an initiation factor protein (eIF4E). This protein recruits other factors that assemble the ribosome on the mRNA in a stepwise process (*1*). In contrast, internal initiation of translation does not require a cap or recognition of the mRNA 5′ end. Rather, structured RNA sequences called internal ribosomal entry sites (IRESs) recruit and activate the translation machinery, functionally replacing many protein factors (*2*). IRESs are essential for infection by many medically and economically important viruses such as hepatitis C (HCV), hepatitis A, polio, foot-and-mouth disease, rhinovirus, coxsackievirus-B3, and HIV-1 (*3*). IRESs also drive the translation of eukaryotic mRNAs, encoding factors involved in development, growth regulation, apoptosis, transcription, translation, and other important cellular processes (*3*). The molecular rules underlying this RNA structure–driven mechanism remain elusive.

Department of Biochemistry and Molecular Genetics, University of Colorado at Denver and Health Sciences Center, Mail Stop 8101, Post Office Box 6511, Aurora, CO 80045, USA.

*To whom correspondence should be addressed. E-mail: Jeffrey.Kieft@uchsc.edu

Ideal model systems for understanding IRES RNA-driven translation are the mechanistically streamlined intergenic region (IGR) IRESs of the virus family Dicistroviridae (*4*). The IGR IRESs drive the association of the ribosomal subunits without any of the protein factors that comprise the canonical translation initiation apparatus (Fig. 1A) (*5*). Hence, this one structured RNA (molecular size ~66 kD) supplants over 1000 kD of structured initiation factor proteins, operating as an all-RNA translation initiation apparatus (*6–9*). The full-length IGR IRES folds in solution into two structurally independent domains (*10–13*). The larger domain (regions 1 and 2, Fig. 1A and fig. S1) is the ribosome-binding domain. It folds into a compact structure (*10*) that binds directly to the 40*S* subunit (*10*, *12*, *13*). Cryo–electron microscopy (cryo-EM) reconstructions of an IGR IRES bound to the ribosome reveal that the IGR IRES binds over the mRNA-binding groove, making contact to and changing the structure of both ribosomal subunits (40*S* and 60*S*) (*14*). However, these cryo-EM structures do not reveal the structure of the IRES, how the IRES structure creates a ribosome-binding site, or which IRES structural features specifically contact and manipulate the ribosome.

To address these questions and develop a model for the structural basis of IGR IRES-driven translation, we have solved the structure of the ribosome-binding domain of the *Plautia stali* intestine virus (PSIV) IGR IRES